

# Empirical Molecular Dynamics: Possibilities, Requirements, and Limitations

Kurt Scheerschmidt

Max Planck Institute of Microstructure Physics, Weinberg 2, D-06120 Halle,  
Germany  
[schee@mpi-halle.de](mailto:schee@mpi-halle.de)

**Abstract.** Classical molecular dynamics enables atomistic structure simulations of nanoscopic systems to be made. The method is extremely powerful in solving the Newtonian equations of motion to predict static and dynamic properties of extended particle systems. However, to yield macroscopically relevant and predictive results, suitable interatomic potentials are necessary, developed on ab-initio-based approximations. The fundamental requirements for performing classical molecular dynamics are presented as well as the relation to statistical methods and particle mechanics, suitable integration and embedding techniques, and the analysis of the trajectories. The applicability of the technique is demonstrated by calculating quantum-dot relaxations and interaction processes at wafer-bonded interfaces.

## 1 Introduction: Why Empirical Molecular Dynamics?

Classical molecular dynamics (MD) enable atomistic structure simulations of nanoscopic systems and are, in principle, a simple tool to approach the many-particle problem. For given interatomic or intermolecular forces one has to integrate the Newtonian equations of motion assuming suitable boundary conditions for the box containing the model structure. There are at least two advantages of this technique. The molecular dynamics is deterministic and provides the complete microscopic trajectories, i.e., the full static and dynamic information of all particles is available, from which a large number of thermodynamic and mechanically relevant properties of the models can be calculated. Further, one can perform simulations that are macroscopically relevant with the present computational power of even desktop computers. With reasonable computational effort models of nanoscale dimension can be treated for several million particles and up to microseconds of real time. Thus, empirical MD has two main fields of application: The search for the global energetic minima by relaxing nanoscopic structures and the calculation of dynamical parameters by analyzing the lattice dynamics.

Computer simulations are performed on models simulating the reality by using approximations, reduction, localization, linearization, etc., the validity of which has to be critically evaluated for each problem considered. As sketched in Fig. 1, increasing the time and length scales of the models (which is necessary to increase the macroscopic validity and robustness of the calculations) requires an increasing number of approximations and thus leads

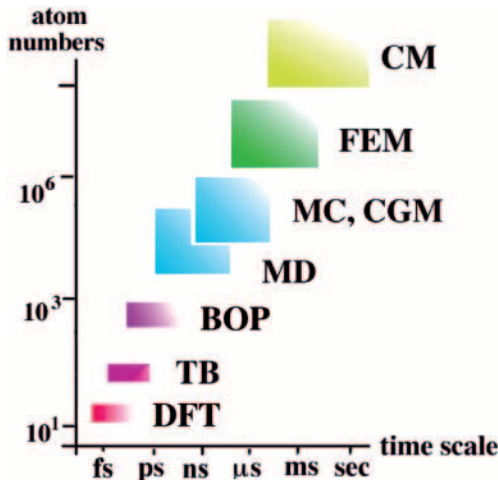


**Fig. 1.** Length and timescales in various modeling methods: DFT = density-functional theory, TB = tight-binding approximations, BOP = bond-order potentials, MD = empirical molecular dynamics, MC, CGM = Monte-Carlo/conjugate-gradient techniques, FEM = finite element methods, CM = continuum mechanics

to a reduction in the ability to predict some physical properties. Density-functional theory (DFT) and its approximations (e.g., local-density LDA, generalized gradient GGA), and the different kinds of tight-binding treatments (TB) up to the bond-order potential (BOP) approximations start with the Born–Oppenheimer (BO) approximation, thus decoupling the ionic and electronic degrees of freedom. Additional approximations such as pseudopotentials, gradient corrections to the exchange-correlation potential, and incomplete basis sets for the single-particle states are required for DFT calculations. The specifics of the various methods are discussed in various Chapters in the present book and in a number of review articles on DFT, TB, linear scaling techniques and programs such as SIESTA and CASTEP [1–9]. In first-principle MD [10], e.g., using DFT or DFT-TB, the electronic system is treated as parameter free and the resulting Hellmann–Feynman forces are the glue of the ionic interactions. Such simulations are computationally too expensive for large systems.

Figure 1 shows that the empirical MD closes the gap between first-principles, macroscopic, and continuum techniques (FEM = finite element methods, CM = continuum mechanics). The latter neglect the underlying interatomic interactions but allow the description of defects, defect interactions, diffusion, growth processes, etc. Stochastic Monte Carlo techniques (MC) enable the further increase of the timescales, also at the first-principles level, but without access to the dynamics. On the other hand, static energy minimization (e.g., conjugate gradient methods, CGM) enable a drastic increase in the model size. However, this does not necessarily provide the global mini-

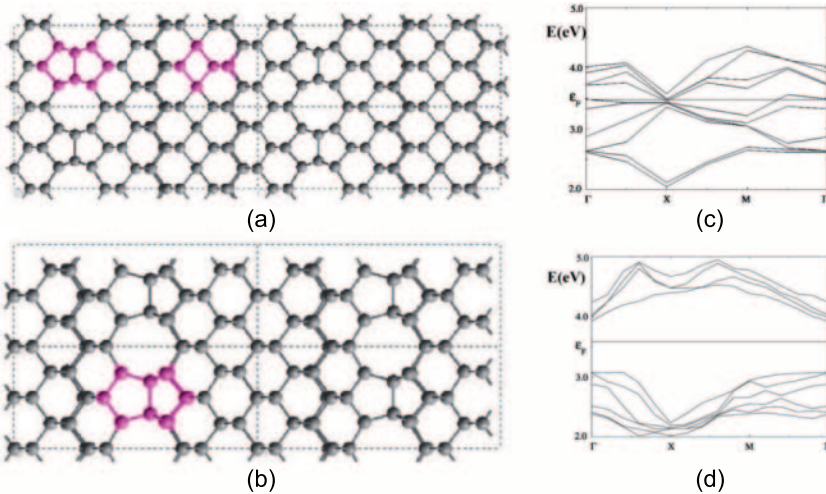


**Fig. 2.** Interface structures at  $90^\circ$  twist boundaries ((a): *Pmm(m)*-layer, (b): *42m-dreidl*, cf. text in Sect. 4.2), predicted by empirical MD and revealed by ab-initio DFT simulations yielding semimetallic/isolating behavior as a function of the interface bonding state as demonstrated by the corresponding DFT band structures (c) and (d), respectively

mum of the potential energy surface. The largest model dimensions (number of atoms) accessible to empirical MD (or MC, CGM) has approximately the same extension as the smallest devices in microelectronics and micromechanics. Thus, today's atomistic modeling approaches the size of actual nanoscale systems.

The assumption of the existence, validity, and accuracy of known empirical interatomic potentials or force fields in analytic form always ignores the underlying electronic origin of the forces, i.e., the quantum structure of the interactions (cf. Sect. 2.4). Therefore, it is important to have better approximations, such as the bond-order potential (BOP), which is developed from tight-binding approximations and discussed briefly in Sect. 3.2. Other possibilities to include electronic properties of the interaction consist in continuously refitting an empirical potential during the calculation, called *learning on the fly* (see Chap. 9 and [11]). Separated subsystems can be treated at an ab-initio level. Suitable handshaking methods can be designed to bridge the embedded subsystem with its surrounding, which is treated semiclassically (cf. [12–15]). However, well-constructed potentials describing sufficiently accurate physical properties also give physical insights and enable a thorough understanding of the underlying processes [2].

Figure 2 shows a simple example demonstrating the difference in the approximation levels. Using empirical MD the correct structural relaxation of special interfaces created by wafer bonding can be treated, as described later

in Sect. 4.2. Two configurations exist, a metastable one (Fig. 2a) and the global minimum structure shown in Fig. 2b, called *dreidl* [16]. The electronic properties demand ab-initio level simulations, done here using a smaller periodic subunit of the interface and applying DFT techniques. It is shown that the higher-level approximation reproduces the structure predicted by the semiempirical techniques, whereas the correct energies and electronic properties (the band structure and the semimetallic or isolating behavior of the interfaces as shown in Figs. 2c,d) can only be described using the DFT formalism.

A second kind of embedding problem occurs because even millions of particles only describe a small part of reality that, even for smaller pieces of matter, is characterized by Avogadro's number ( $6 \times 10^{23} \text{ mol}^{-1}$ ). Since isolated systems introduce strong surface effects, each model has to be embedded in suitable surroundings. For a discussion of various types of boundary conditions, see Sect. 3.1, Chap. 9 and [13–15].

The fundamental requirements of classical MD simulations, the relation to statistical methods and particle mechanics, suitable integration and embedding techniques and the analysis of the trajectories are presented in Sect. 2. The enhancements of potentials (bond-order potentials) and boundary conditions (elastic embedding) are discussed in Sect. 3. Selected application of semiempirical MD (relaxation of quantum dots and wafer-bonded interfaces) are given in Sect. 4 together with some examples from the literature. They strongly depend on the approximations assumed in the simulations.

## 2 Empirical Molecular Dynamics: Basic Concepts

The main steps for applying empirical molecular dynamics consist of the integration of the basic equations (cf. Sect. 2.1) using a suitable interaction potential and embedding the model in a suitable surrounding (cf. Sect. 2.4 and Sect. 2.3, respectively). Textbooks of classical molecular dynamics, e.g., [17–23], describe the technical and numerical details, and provide a good insight into possible applications and the physical properties, which may be predictable. Here, only the main ideas of empirical MD simulations, viz. the basic equations, methods of numerical treatment and the analysis of the trajectories are discussed.

### 2.1 Newtonian Equations and Numerical Integration

The basic equations of motion solved in empirical MD are the Newtonian equations for  $N$  particles ( $i = 1, \dots, N$ ) characterized by their masses  $m_i$ , their coordinates  $\mathbf{r}_i$ , and the forces acting on each particle  $\mathbf{f}_i$ . These may include external forces  $\mathbf{F}_i$  and interatomic interactions  $\mathbf{f}_i = \sum_{j \neq i} \mathbf{f}_{ij}$ :

$$m_i \ddot{\mathbf{r}}_i = \mathbf{f}_i = -\frac{\partial \mathcal{V}(\mathbf{r}_1, \mathbf{r}_2, \dots, \mathbf{r}_N)}{\partial \mathbf{r}_i}. \quad (1)$$

The assumption that a potential  $\mathcal{V}$  exists presupposes conservative (nondissipative) interactions and needs some more general considerations, cf. Sect. 2.2. If one assumes pairwise central potentials,  $\mathcal{V}(\mathbf{r}_1, \mathbf{r}_2, \dots, \mathbf{r}_N) = \sum'_{i,j} \mathcal{V}(r_{ij})$  with  $r_{ij} = |\mathbf{r}_j - \mathbf{r}_i|$  (the dash means that the sum is restricted to  $i < j$ ), it follows that the virial of the external and internal forces is  $\mathcal{M} = \sum'_{i,j} \mathbf{r}_{ij} \mathbf{f}_{ij} = \sum_i \mathbf{r}_i \mathbf{F}_i$ . If the system is isolated (microcanonical ensemble), the conservation of total energy  $\mathcal{E} = \mathcal{K} + \mathcal{V}$  (with kinetic energy  $\mathcal{K} = \sum_i m_i \dot{\mathbf{r}}_i^2$ ) is guaranteed:

$$\dot{\mathcal{E}} = \dot{\mathcal{K}} + \dot{\mathcal{V}} = \sum_i m_i \dot{\mathbf{r}}_i \cdot \ddot{\mathbf{r}}_i - \sum_i \dot{\mathbf{r}}_i \mathbf{f}_i = 0. \quad (2)$$

Given an initial configuration of particles and suitable boundary conditions (cf. Sect. 2.3), the differential equations can be integrated using one of the standard methods, e.g., Runge–Kutta techniques, predictor–corrector methods, Verlet or Gear algorithm. The numerical integration is equivalent to a Taylor expansion of the particle positions  $\mathbf{r}_i(t + \delta t)$  at a later time in terms of atomic positions  $\mathbf{r}_i$  and velocities  $\mathbf{v}_i$ . The forces  $\mathbf{f}_i$  are the time derivatives of  $\mathbf{r}_i$  with an increasing order at previous time steps:

$$\mathbf{r}_i(t + \delta t) = \mathbf{r}_i(t) + a_1 \delta t \mathbf{v}_i(t) + a_2(\delta t)^2 \mathbf{f}_i(t) + \dots + \mathcal{O}(\delta t^n). \quad (3)$$

In addition to good potentials and system restrictions (cf. Sect. 2.3 and Sect. 2.4, respectively) an efficient and stable integration procedure is required to accurately propagate the system. The conservation of energy during the simulation is an important criterion. An increase in order allows larger time increments  $\delta t$  to be used, if the evaluation of the higher derivatives is not too time consuming, which happens with more accurate potentials, like the BOP (Sect. 3.2). The efficiency and the accuracy of the integration can be controlled by choosing suitable series-expansion coefficients  $a_j, j = 1, 2, \dots, n - 1$  and the order  $n$  of the method or by mixing the derivatives of  $\mathbf{r}_i$  at different times in (3) to enhance the procedure. However, the increment  $\delta t$ , of the order of fs, must be at least so small that the fastest particle oscillations are sufficiently sampled.

Better or faster MD calculations may be performed using special acceleration techniques, the three most important methods being:

1) Localization: By using the linked-cell algorithm and/or neighbor lists, it is assumed that for sufficiently rapidly decaying potentials (faster than Coulomb  $1/r$  for  $r \rightarrow \infty$ ) only a small number of particles have a direct and significant interaction. A cutoff  $r_c$  is defined and the interaction potential is assumed to be zero for  $r > r_c$ . A transition region is fitted using splines or other suitable functions. Then the system is divided into cells. Their minimum dimension is given by  $2r_c$  to avoid self-interaction of the particles (*minimum image convention*). Only the interactions of the atoms within a cell and its 26 neighboring cells are considered, which reduces the simulation time drastically from the  $\propto N^2$  behavior for all particle interactions to linear behavior  $\propto 729c_N N$ , where  $c_N$  is the average number of particles per cell.

The problem is to find a suitable  $r_c$  for a smooth transition and screening behavior that includes a sufficient number of next-neighbor atoms and cells. One also needs a suitable criterion to update the neighbor lists and reorder the cells whenever particles leave a cell during the propagation of the system.

The Coulomb potential may also be screened. However, summations over the long-range  $1/r$  potential, representing infinite point-charge distributions, are only conditionally convergent. Thus, it is better to apply the Ewald method (originally developed to calculate cohesive energies and Madelung constants [24]) and its extensions [25, 26] based on successive charge neutralization by including next-neighbor shells around the origin.

2) Parallelization: Using replicas, or dividing the structure into several parts, which are then distributed to different processors, thus allowing parallelization [27, 28]. The replica technique needs suitable criteria for dividing the system into small parts with minimum interaction. More importantly, one must bear in mind that the replicas are not independent over long times. A careful control of the time interval after which the communication between the different parts is required in order to achieve the same results as nonparallelized simulations. This issue is the bottleneck of the technique.

3) Time stretching: Such techniques as hyperdynamics, temperature acceleration, basin-constrained dynamics, on-the-fly Monte-Carlo, and others are subsumed briefly here, because their common idea consists in replacing the true time evolution by a shorter one increasing the potential minima, transition frequencies, system temperature, etc. (see [28]).

## 2.2 Particle Mechanics and Nonequilibrium Systems

In classical mechanics a system is characterized either by its Lagrangian  $\mathcal{L}(q, \dot{q}) = \mathcal{K}(q, \dot{q}) - \mathcal{V}(q)$  or its Hamiltonian related to the Lagrangian by a Legendre transform  $\mathcal{H}(q, p) = \sum \dot{q}_i p_i - \mathcal{L} = \mathcal{K} + \mathcal{V}(q)$ , where  $q_i, p_i$  are generalized coordinates and momenta (conjugate coordinates), respectively, which have to be independent or unrestricted. One derives the generalized momenta from the derivatives of the Lagrangian  $p_i = \frac{\partial \mathcal{L}}{\partial \dot{q}_i}$ , whereas the derivatives of the Hamiltonian

$$\dot{q}_i = \frac{\partial \mathcal{H}}{\partial p_i}, \quad \dot{p}_i = -\frac{\partial \mathcal{H}}{\partial q_i} \quad (4)$$

reproduce Newton's law of motion (1).

Hamilton's principle of least action enables a simple generalization of the mechanics of many-particle systems. The integral over the Lagrangian function has to be an extremum. Variational methods yields, applying the extremal principle:

$$\frac{d}{dt} \frac{\partial \mathcal{L}}{\partial \dot{q}_i} - \frac{\partial \mathcal{L}}{\partial q_i} = 0. \quad (5)$$

The advantage of the general formulation (5) is that it allows a simple extension to nonconservative systems by including an explicit time dependence or to systems with constraints, such as fixed bond lengths in subsystems, friction of particles, outer forces, etc. If there are holonomic constraints describing relations between the coordinates  $f_l(\mathbf{q}_k) = 0$ , one gets the generalized additional coordinates  $a_{lk} = \partial f_l / \partial q_k$  and  $a_l = \partial f_l / \partial t$  creating an additional term on the right-hand side of (5) in the form  $\sum_l \lambda_l a_{lk}$  with the set of Lagrange multipliers  $\lambda_l$ . This formalism is the basis for the enhancement of the boundary conditions in Sect. 3.1 and the handshaking methods mentioned above.

In addition, the Lagrangian and Hamiltonian formalisms correlate classical dynamics to statistical thermodynamics and to quantum theory, and allow the evaluation of properties from the trajectories (cf. Sect. 2.5). The set of time-dependent coordinates  $\mathbf{q}$  (the configuration space) and time-dependent momenta  $\mathbf{p}$  (momentum space) together is called the phase space  $\Gamma = (\mathbf{q}, \mathbf{p}) = (q_1, q_2, \dots, q_n, p_1, p_2, \dots, p_n)$ . Presenting  $\Gamma$  in a 6-dimensional hyperspace yields  $N$  trajectories, one for each molecule, and allows the study of the behavior of the system using statistical methods. It is called the  $\mu$ -space (following Ehrenfest) or the Boltzmann molecule phase space. The whole  $\Gamma$ -set as one trajectory in a  $6N$ -dimensional hyperspace presents the Gibbs phase space, with the advantage to include better interactions and restrictions. However, the system must now be described as a virtual assembly for statistical relations. The phase space  $\Gamma$  contains the complete information on the microscopic state of the many-particle system. Several basic quantities may be derived such as the phase-space flow or the “velocity field”  $\dot{\Gamma} = (\dot{\mathbf{q}}, \dot{\mathbf{p}})$ . Applying the relations (4) yields the Liouville equation

$$\nabla_\Gamma \Gamma = \sum \left( \frac{\partial \dot{\mathbf{q}}_i}{\partial \mathbf{q}_i} + \frac{\partial \dot{\mathbf{p}}_i}{\partial \mathbf{p}_i} \right) = 0, \quad (6)$$

showing that the flow  $\dot{\Gamma}$  behaves like an incompressible liquid, i.e., although the  $\mu$ -trajectories are independent, their related phase-space volume is constant.

An equivalent formulation of the Liouville statement (6) is the equation of continuity for  $\dot{\Gamma}$ ,  $\dot{\rho}$ , and the local change of the density  $\rho(\mathbf{q}, \mathbf{p}, t)$ , similar to the Heisenberg equation for observables in quantum theory. The density  $\rho(\mathbf{q}, \mathbf{p}, t)$  describes the probability of finding the system within the region  $\mathbf{p}, \mathbf{q}$  and  $\mathbf{p} + d\mathbf{p}, \mathbf{q} + d\mathbf{q}$  of the phase-space volume  $d\mathbf{p}d\mathbf{q}$ . Because the systems must be somewhere in the phase space, the density can be normalized in the entire phase space. The integral over the whole phase space of the non-normalized density yields the partition function. Integration over  $(N - k)$  particles yields the  $k$ -particle phase-space density  $\rho^{(k)}(\mathbf{q}, \mathbf{p}, t) = \int \rho^{(N)}(\mathbf{q}, \mathbf{p}, t) d\mathbf{p}^{(N-k)} d\mathbf{q}^{(N-k)}$ , and the integration over the whole momentum space the corresponding  $k$ -particle distribution function  $n^{(k)}(\mathbf{q}) = \int \rho^{(N)}(\mathbf{q}, \mathbf{p}, t) d\mathbf{q}^{(N-k)} d\mathbf{p}$ . Very important for the trajectory analy-

sis (Sect. 2.5) are the cases  $k = 1, 2$  defining the (radial) pair-distribution functions  $g(\mathbf{q}_i, \mathbf{q}_j)$ :

$$n^{(1)}(\mathbf{q}_i)n^{(1)}(\mathbf{q}_j)g(\mathbf{q}_i, \mathbf{q}_j) = n^{(2)}(\mathbf{q}_i, \mathbf{q}_j). \quad (7)$$

The phase-space trajectories allow the classification of the dynamics of many-particle systems. They may be Poincare-recurrent (the same phase-space configuration occurs repeatedly), Hamiltonian (nondissipative), conservative (no explicit time dependence for the Hamiltonian), or integrable (number of constants of motion equals the number of degrees of freedom, resulting in stable periodic or quasiperiodic systems). Nonintegrable systems may be ergodic or mixing, etc., i.e., the trajectory densely covers different hypersurfaces in the phase space, and allow the characterization of different kinds of instabilities of the system.

### 2.3 Boundary Conditions and System Control

As mentioned above, even for systems considered large in MD simulations, the number of atoms is small compared to real systems and therefore dominated by surface effects. They are caused by interactions at free surfaces or with the box boundaries. In order to reduce nonrealistic surface effects, periodic boundary conditions are applied, or the box containing the model (supercell) has to be enlarged so that the influence of the boundaries may be neglected. For further discussion and enhancements including elastic embedding, see Sect. 3.1. Periodic boundary conditions means that the supercell is repeated periodically in all space directions with identical image frames or mirror cells. In contrast to the case of fixed boundaries, under periodic boundary conditions the particles can move across the boundaries. If this happens, the positions  $\mathbf{r}$  have to be replaced by  $\mathbf{r} - \boldsymbol{\alpha}$  where  $\boldsymbol{\alpha}$  is a translation vector to the image frame to which the particle is moved. Particle number, total mass, total energy, and momenta are conserved in periodic boundary conditions, but the angular momenta are changed and only an average of them is conserved. It should be mentioned here that periodic boundary conditions repeat defects, which in small supercells create high defect concentrations. Antiperiodic and other special boundary conditions may be chosen, where additional shifts of the positions and momenta along the box borders allow correction of a disturbed periodic continuation and a description of reflective walls at free surfaces to be obtained.

According to the boundary conditions and system restrictions, the virtual Gibbs entities are either isolated microcanonical ensembles with constant volume, total energy, and particle numbers ( $NVE$  ensembles) or systems that exchange and interact with the environment. Closed ensembles (e.g., canonical  $NVT$  or isothermic-isobar  $NPT$  systems) have only an energy exchange with a thermostat, whereas open systems have in addition particle exchange with the environment (e.g., grand-canonical  $T\mu V$ , where  $\mu$  is the chemical potential).

Simple tools exist to equilibrate systems at a well-defined temperature. For example, velocity rescaling is numerically equivalent to a simple extension of the original microcanonical system with nonholonomic constraints in the Lagrangian formalism and is called the Berendsen thermostat. A similar simple extension may be used for pressure rescaling. It is called the Berendsen barostat [29]. The simple velocity rescaling works by conserving the Maxwell distribution and yielding maximum entropy. However, such nonisolated ensembles are better described using constraints in the Lagrangian similar to those discussed in Sect. 2.2. The extension of  $\mathcal{L}$  in (5) by adding terms  $\mathcal{L}_{\text{constr}}$  introduces additional generalized variables having extra equations of motion and also additional force terms in the Newtonian equations (1). Some of the most important methods for  $\mathcal{L}_{\text{constr}}$  are given below without further comments:

- Nosé–bath and generalized Nosé–Hoover thermostat [30–32]:  $\mathcal{L}_{\text{constr}} = M\dot{s}^2/2 - n_f T \ln(s)$  with the fictive or the whole mass  $M = \sum m_i$ , the degrees of freedom  $n_f = 3N + 1$ , and the new generalized variable  $s$  playing the role of an entropy.
- Andersen isothermal-isobaric system control (NPH ensemble)  $\mathcal{L}_{\text{constr}} = \dot{V}^2/2 + PV$  introduces volume and pressure as generalized variables [33].
- Generalized stresses according to Parrinello and Rahman [34]  $NTL\sigma$ -ensembles: the Lagrangian is extended by  $\mathcal{L}_{\text{constr}} = -1/2Tr\boldsymbol{\Sigma}\mathbf{G}$  with a generalized symmetric tensor  $\boldsymbol{\Sigma}$  and the metric tensor  $\mathbf{G}$  of the crystal structure. A further specialization, e.g., for constant strain rates  $NTL_x\sigma_{yy}\sigma_{zz}$ -ensemble [35], is in principle a mixture of the isothermal-isobaric system with the generalized stress constraint.
- Brownian fluctuations, transport and flow processes, density and other gradients, Langevin damping  $\propto \mathbf{v}(t)$ , etc. demand nonequilibrium MD [36, 37], which is mostly done by including the perturbation as a suitable virtual field  $\mathcal{F}(\mathbf{p}, \mathbf{q}, t)$  into the equations of motion via the Lagrange formalism.

## 2.4 Many-Body Empirical Potentials and Force Fields

Empirical potentials and force fields exist with a wide variety of forms, and also different classification schemes are used according to their structure, applicability, or physical meaning. It makes no sense to describe a large number of potentials or many details in the present review, therefore only some of the existing and most used potentials are briefly listed below (a good overview can be found in [38–48]. A classification by Finnis [2] (and many references therein) describes recent developments and discusses in an excellent way the justification of the potentials by first-principle approximations, which is important for the physical reliability and the insight into the electronic structure of potentials. Interatomic forces are accurate only if the influence of the local environment according to the electronic structure is included. The most

important property of a potential is transferability, that is the applicability of the potential to varied bonding environments. An important additional criterion is its ability to predict a wide range of properties without refitting the parameters. The number of fit parameters decreases as the sophistication of the force fields increases. According to [2] one has:

*Pair potentials* – Valid for *s-p* bonded metals and mostly approximated by a sum of pairwise potentials. They may be derived as the response to a perturbation in jellium, which can be visualized in the pseudoatom picture as an ionic core and a screening cloud of electrons.

*Ionic potentials* – To use Coulomb interactions directly for ionic structures, the problem of screening (Ewald summation, Madelung constant) has to be considered as mentioned above. The interactions were originally described by Born and others as the rigid-ion approximation. Starting from the Hohenberg–Kohn–Sham formulation of the DFT-LDA, shell or deformable ion models may be developed beyond the rigid-ion approximation, where the additional shell terms [49] look like electron-density differences in noble gases.

*Tight-binding models* – Different derivations and approximations for TB-related potentials exist and are nowadays applicable to semiconductors, transition metals, alloys and ionic systems. The analytic bond-order potential is such an approximation and will be discussed in more detail in Sect. 3.2.

*Hybrid schemes* – Combinations of pair potentials with TB approximations are known as generalized pseudopotentials, effective media theories (EMT [50]), environmental-dependent ionic potentials (EDIP [51]), or embedded atom models (EAM [52]); for details see [2].

From the empirical point of view the simplest form of potentials may be considered to be a Taylor-series expansion of the potential energy with respect to 2-, 3-,...,  $n$ -body atomic interactions. Pair potentials have a short-range repulsive part, and a long-range attractive part, e.g., of the Morse or Lennard–Jones (LJ) type, mostly “12–6”, i.e.,  $ar^{-12} - br^{-6}$ . LJ potentials are successfully applied to noble gases, biological calculations, or to model long-range van der Waals interactions (e.g. [53]). For quasicrystals [54] an LJ potential was constructed with two minima in a golden number distance relation. However, simple pair potentials are restricted in their validity to very simple structures or to small deviations from the equilibrium. Therefore many-body interactions are added and fitted for special purposes, e.g., the MD of molecules and molecule interactions [55, 56]. Separable 3-body interactions are widely used: Stillinger–Weber [57] (SW), Biswas–Hamann [58], and Takai–Halicioglu–Tiller [59] potentials. The SW is perhaps the best-known 3-body-type potential. It includes anharmonic effects necessary to reproduce the thermal lattice expansion of Si and Ge [60]. Hybrid force fields are sometimes used to include the interaction of different types of atoms, such as Born–

Mayer–Huggins, Rahmann–Stillinger–Lemberg terms and others applicable to silicate glasses and interdiffusing metal ions or water molecules [61–65].

As mentioned above, other force fields are developed from first-principle approximations that combine sufficient simplicity with high rigor. They are not based upon an expansion involving  $N$ -body interactions (cluster potentials). The more or less empirical forms of TB potentials and effective medium force fields are the modified embedded atom model (MEAM, [66] for cubic structures and references therein for other structures), the Finnis–Sinclair (FS) [67] and the Tersoff-type (TS) potentials [68–70]. The TS potential is an empirical bond-order potential with the functional form:

$$V(\mathbf{r}_{ij}) = ae^{-\lambda \mathbf{r}_{ij}} - b_{ij}e^{-\mu \mathbf{r}_{ij}}. \quad (8)$$

The bonds are weighted by the bond order  $b_{ij} = F(\mathbf{r}_{ik}, \mathbf{r}_{jk}, \gamma_{ijk})$  including all next neighbors  $k \neq i, j$ , which gives the attractive interaction the form of an embedded many-body term. The different parameterizations (TI, TII, TIII) of the Tersoff potential have been intensively tested. Other parameterizations exist [71]. They involve other environmental functions and first-principle derivations [72, 73], as well as extensions to include further interactions, H in Si [74], C, Ge [75], C–Si–H [76, 77], AlAs, GaAs, InAs, etc. [78]. Finally, a refitted MEAM potential with SW terms is available for Si [79]. Multipole expansions replaced by spherical harmonics [80] are an alternative to TS potentials.

A comparative study of empirical potentials shows advantages and disadvantages in the range of validity, physical transparency, fitting and accuracy as well as applicability [81]. Restrictions exist for all empirical potential types, even if special environmental dependencies are constructed to enhance the elastic properties near defects. In addition, not all potentials are applicable to long-range interactions, and the electronic structure and the nature of the covalent bonds can only be described indirectly. Thus, it is of importance to find physically motivated semiempirical potentials, as mentioned above and discussed in Sect. 3.2 for TB-based analytic BOPs. The parameters of the empirical force field have to be fitted to experimental data or first-principle calculations. First, the cohesive energy, lattice parameter and stability of the crystal structures have to be tested or fitted. The bulk modulus, elastic constants, and phonon spectra are very important properties for the fit. The following section describes some of the quantities that may be used for the fit or to be evaluated from the MD simulations if not fitted. Very important details concerning point defects and defect clusters – necessary to get the higher-order interaction terms – are given by the energy and structure of such defects. The data may be given by DFT or TB dynamics or geometry optimizations, as, e.g., [82–85].

## 2.5 Determination of Properties

Static properties of systems simulated by empirical MD can be directly calculated from the radial- or pair-distribution function (7). Dynamic properties follow from the trajectories using averages or correlations:

$$\langle A \rangle_t = \lim_{t \rightarrow \infty} \frac{1}{t - t_0} \int_{t_0}^t dt A[\mathbf{r}(t)], \quad C(t) = \langle A(\tau)B(t + \tau) \rangle_\tau, \quad (9)$$

which in principle correspond to time averages. However, they are sampled at discrete points, so that it is necessary to choose suitable sampling procedures to reduce the effects of the finite size of the system, stochastic deviations, and large MD runs.

Two basic relations are central for the analysis of the properties. The ergodic hypothesis states that the ensemble average  $\langle A \rangle_e$  is equal to the time average  $\langle A \rangle_t$ , which relates the averages to the measurement of a single equilibrium system. The Green–Kubo formula  $\lim_{t \rightarrow \infty} \frac{\langle [A(t) - A(t_0)]^2 \rangle_t}{t - t_0} = \int_{t_0}^\infty d\tau \langle \dot{A}(\tau) \dot{A}(t_0) \rangle_e$  relates mean square deviations with time correlations. The diffusion coefficient  $D = \lim_{t \rightarrow \infty} \frac{1}{6Nt} \langle \sum_j [\mathbf{r}_j(t) - \mathbf{r}_j(0)]^2 \rangle$  (Einstein relation) is equivalent to the velocity autocorrelation function, which is a special form of the Green–Kubo formula  $D = \frac{1}{3N} \int_0^\infty \langle \sum_j \mathbf{v}_j(t) \cdot \mathbf{v}_j(0) \rangle$ . Similarly, one uses the crosscorrelation of different stress components to obtain shear viscosities. Other transport coefficients may be derived analogously.

In thermodynamic equilibrium the kinetic energy  $\mathcal{K}$  per degree of freedom is determined by the equipartition theorem  $\mathcal{K} = \langle \sum_i m_i \dot{v}_i^2 / 2 \rangle = 3Nk_B T / 2$  ( $k_B$  = Boltzmann constant) which yields a measure of the system temperature  $T$ . The strain tensor  $\sigma$  and the pressure  $P$  are obtained from the generalized virial theorem  $\sigma_{kl} = 1/V [\sum_j \mathbf{v}_{jk} \cdot \mathbf{v}_{jl} + \sum_{ij} \mathbf{r}_{ijk} \cdot \mathbf{f}_{ijl}]$ . Thus, the pressure is the canonical expectation value  $P = 1/3V[2\mathcal{K} - \mathcal{M}]$  of the total virial  $\mathcal{M}$ . Alternatively, one can use the pair distribution in the form  $P = \rho k_B T - \rho^2 \int_0^\infty g(r) \frac{\partial U}{\partial r} 4\pi r^3 dr$ , which may be useful for correcting sampling errors.

Using the densities  $\rho(\mathbf{r}, \mathbf{p})$  as defined above and  $\mathcal{Z} = \int \rho(\mathbf{r}, \mathbf{p}) d\mathbf{r}$  as normalization, statistical mechanics deals with ensemble averages, which in general are written as

$$\langle Q \rangle_e = 1/\mathcal{Z} \int Q(\mathbf{r}, \mathbf{p}) \rho(\mathbf{r}, \mathbf{p}) d\mathbf{r}. \quad (10)$$

All thermodynamic functions may be derived from the partition function  $\mathcal{Z}$ , for example the free energy  $F(T, V, N) = -k_B T \ln[\mathcal{Q}(T, V, N)]$ . In addition, one can obtain all the thermodynamic response coefficients. With the internal energy  $U$ , one computes the isochoric heat capacity  $C_V = (\partial U / \partial T)_{N,V}$  and thus a measure for the quality of the temperature equilibration  $(\langle T \rangle^2 - \langle T^2 \rangle) / \langle T^2 \rangle = 3/2N(1 - 3kN)/2c_V$ . From the volume  $V$  follows the isothermal compression  $\chi_T = -1/V(\partial V / \partial P)_{N,T}$ , etc. One has to choose according to the different ensembles:

- Microcanonical:  $\rho_{NVE} = \delta[\mathcal{H}(\mathbf{r}, \mathbf{p}) - \mathcal{E}]$  conserving entropy  $S(E, N, V)$ .
- Canonical:  $\rho_{NVT} = e^{(\mathcal{H}/k_B T)} \propto e^{V(\mathbf{r})/k_B T}$  conserving free energy  $F(T, V, N)$
- Isothermic-isobaric:  $\rho_{NPT} = e^{(\mathcal{H}-TS)/k_B T}$  conserving Gibbs free energy  $G(T, P, N)$
- Grand canonical:  $\rho_{T\mu V} = e^{(\mathcal{H}-\mu N)/k_B T}$  conserving Massieu function  $J(T, \mu, V)$  (Legendre transformation in entropy representation).

Finally, it should be mentioned that the Fourier transform of pair distributions is connected to the scattering functions in X-ray, neutron and electron diffraction. MD-relaxed structure models allow the simulation of the transmission electron microscope (TEM) or high-resolution electron microscope (HREM) image contrast and therefore make the contrast analysis more quantitative. For this purpose, snapshots of the atomic configurations are cut into thin slices, which are folded with atomic scattering amplitudes and each other to describe the electron scattering (multislice formulation of the dynamical scattering theory), cf. the applications in Sect. 4 using this technique to interpret HREM investigations of quantum dots and bonded interfaces.

### 3 Extensions of the Empirical Molecular Dynamics

Coupling of length and timescales in empirical MD means bridging the first-principles particle interactions and the box environment (1). It can be done either using embedding and handshaking or by a separate treatment and a transfer parameter between the subsystems. MD simulations of the crack propagation [86] and the analysis of submicrometer MEMS [87] are successfully applications of the FEM coupling between MD and an environmental continuum. In Sect. 3.1 enhanced boundary conditions for MD are discussed: where the coupling between MD and an elastic continuum is a handshaking method based on an extended Lagrangian [88, 89]. The main steps in the development of an analytic TB-based BOP [90] are sketched in Sect. 3.2 as an example of using enhanced potentials.

#### 3.1 Modified Boundary Conditions: Elastic Embedding

Elastic continua may be coupled to MD when the potential energy of an infinite crystal with a defect as shown in Fig. 3a is approximated in the outer region II by generalized coordinates  $a_k$  [89]:

$$E(\{\mathbf{r}_i\}, \{\mathbf{r}_j\}) = E(\{\mathbf{r}_i\}, \{a_k\}). \quad (11)$$

In the defect region I, characterized by large strains, the positions of atoms  $\mathbf{r}_i$  ( $i = 1, \dots, N$ ) are treated by empirical MD. The atomic positions  $\mathbf{r}_j$  ( $j > N$ ) in the outer regions II and III result from the linear theory of elasticity

$$\mathbf{r}_j = \mathbf{R}_j + \mathbf{u}^{(0)}(\mathbf{R}_j) + \mathbf{u}(\mathbf{R}_j, \{a_k\}), \quad (12)$$

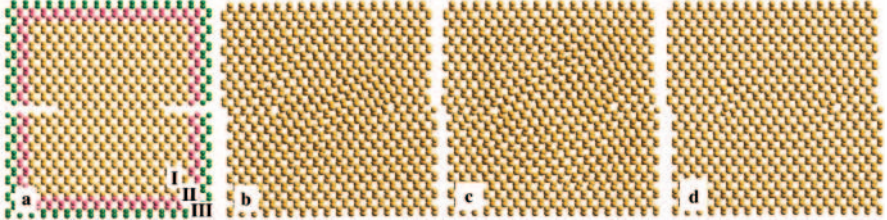


**Fig. 3.** Dislocation geometry ((a), I = MD region, II = elastic, III = overlap, cf. text) to apply elastic boundary conditions for a dipole of  $60^\circ$  dislocations, and snapshots during MD annealing: 500 K (b), 600 K (c), 0 K (d)

where the fields  $\mathbf{u}^0(\mathbf{R})$  and  $\mathbf{u}(\mathbf{R})$  describe the displacements of atoms from their positions  $\mathbf{R}_j$  in the perfect crystal, and satisfy the equilibrium equations of a continuous elastic medium with defects;  $\mathbf{u}^0(\mathbf{R})$  is the static displacement field of the defect and independent of the atomic behavior in I;  $\mathbf{u}(\mathbf{R})$  is related to the atomic shifts in region I and can be represented as a multipole expansion:

$$\mathbf{u}(\mathbf{R}, \{a_k\}) = \sum_{k=1}^{\infty} a_k \mathbf{U}^{(k)}(\mathbf{R}) \quad (13)$$

over homogeneous eigensolutions  $\mathbf{U}^{(k)}(\mathbf{R})$  [88]. The  $\mathbf{U}^{(k)}$  are rapidly decreasing with  $\mathbf{R}$ , thus the sum in (13) is truncated to a finite number  $K$  of terms.

The equilibrium positions of atoms in the entire crystal are obtained from the minimization of the potential energy given in (11) with respect to  $\mathbf{r}_i$  and  $a_k$ . This is equivalent to a dynamic formulation based on the extended Lagrangian as discussed above (Sect. 2.2 and Sect. 2.3) with the extension (11):

$$\mathcal{L} = \sum_{i=1}^N \frac{m_i \dot{\mathbf{r}}_i^2}{2} + \sum_{k=1}^K \frac{\mu \dot{a}_k^2}{2} - E(\{\mathbf{r}_i\}, \{a_k\}). \quad (14)$$

Here,  $m_i$  are the atomic masses and  $\mu$  is a parameter playing the role of mass for the generalized coordinates  $a_k$ . If  $\mu$  is properly chosen, the phonons are smooth from I to II and the outer regions oscillate slower than the MD subsystem as demonstrated in the snapshots Figs. 3b–d. The corresponding system defining the forces reads

$$\mathbf{F}_i = -\frac{\partial E(\{\mathbf{r}_i\}, \{a_k\})}{\partial \mathbf{r}_i}, \quad (15)$$

$$F_k = -\frac{\partial E(\{\mathbf{r}_i\}, \{a_k\})}{\partial a_k} = -\sum_{j>N} \frac{\partial E(\{\mathbf{r}_i\}, \{\mathbf{r}_j\})}{\partial \mathbf{r}_j} \frac{\partial \mathbf{r}_j}{\partial a_k} = \sum_{j \in \text{II}} \mathbf{F}_j \mathbf{U}^{(k)}(\mathbf{R}_j). \quad (16)$$

These must vanish in the equilibrium  $\mathbf{F}_i = F_k = 0$ . The sum in (16) expands only over the atoms in region II surrounding region I, since in region III the linear elasticity alone is sufficient and the forces on these atoms are nearly vanishing. However, region II must be completely embedded in region III. The forces on atoms in region II must be derived from the interatomic potential, therefore the size of region II must be extended beyond the potential cutoff  $r_c$ . The Lagrangian (14) results in the equations of motion

$$m\ddot{\mathbf{r}}_i = \mathbf{F}_i, \quad (i = 1, \dots, N), \quad \mu\ddot{a}_k = F_k, \quad (k = 1, \dots, K), \quad (17)$$

thus extending Newton's equations by equivalent ones for the generalized coordinates.

### 3.2 Tight-Binding-Based Analytic Bond-Order Potentials

As discussed before, the use of TB methods allows much larger models than accessible to DFT. TB formulations exist in many forms (e.g., [2, 6–8, 91–93]). The application of an analytical BOP, developed mainly by *Pettifor* and coworkers [90, 94–98], may further enhance empirical MD by providing better justified force fields while allowing faster simulations than numerical TB-MD. The approximations to develop analytic TB potentials from DFT may be summarized by the following steps (cf. also [2, 99]): 1. Construct the TB matrix elements by Slater–Koster two-center integrals including *s*- and *p*-orbitals, 2. transform the matrix to the bond representation, 3. replace the diagonalization by Lanczos recursion, 4. get the momenta of the density of states from the continued fraction representation of the Green's function up to order  $n$  for an analytic BOP- $n$  potential. The basic ideas sketched with a few more details are as follows.

The cohesive energy of a solid in the TB formulation can be written in terms of the pairwise repulsion  $U_{\text{rep}}$  of the atomic cores and the energy due to the formation of electronic bonds

$$\begin{aligned} U_{\text{coh}} &= U_{\text{rep}} + U_{\text{band}} - U_{\text{atoms}} \\ &= \frac{1}{2} \sum'_{i,j} \phi(r_{ij}) + 2 \sum_{n(\text{occ})} \epsilon^{(n)} - \sum_{i\alpha} N_{i\alpha}^{\text{atom}} \varepsilon_{i\alpha}, \end{aligned} \quad (18)$$

where the electronic energy  $\varepsilon$  of the free atoms has to be subtracted from the energy of the electrons on the molecular orbitals  $\epsilon$ . Replacing  $\epsilon^{(n)}$  with the eigenstates of the TB-Hamiltonian for orbital  $\alpha$  at atom  $i$ ,

$$\epsilon^{(n)} = \epsilon^{(n)} \langle n | n \rangle = \langle n | \epsilon^{(n)} | n \rangle = \langle n | \mathcal{H} | n \rangle = \sum_{i\alpha, j\beta} C_{i\alpha}^{(n)} H_{i\alpha, j\beta} C_{j\beta}^{(n)}, \quad (19)$$

the electronic contributions to the cohesive energy  $U_{\text{band}} - U_{\text{atom}} = U_{\text{bond}} + U_{\text{prom}}$  can be rearranged and separated in the diagonal and offdiagonal parts:

$$U_{\text{bond}} = 2 \sum'_{i\alpha, j\beta} \rho_{j\beta, i\alpha} H_{i\alpha, j\beta}, \quad U_{\text{prom}} = \sum_{i\alpha} [2\rho_{i\alpha, i\alpha} - N_{i\alpha}^{\text{atom}}] \varepsilon_{i\alpha}. \quad (20)$$

The third contribution, the promotion energy  $U_{\text{prom}}$  compares the occupancy of the atomic orbitals of the free atoms with the occupation of the corresponding molecular orbitals [100]. The bond energy  $U_{\text{bond}}$  describes the energy connected with the exchange or hopping of electrons between arbitrary pairs of atomic neighbors  $\{i(j), j(i)\}$ , the factor 2 is due to the spin degeneracy. The transition matrix elements of the Hamiltonian are hopping energies, and their transition probability is given by the corresponding element of the density matrix. The contribution for one bond between the atoms  $i$  and  $j$  is thus characterized by the part of the density called the *bond order*  $\Theta_{j\beta,i\alpha}$  that may be expressed as a trace:

$$U_{\text{bond}}^{i,j} = \sum_{\alpha,\beta} H_{i\alpha,j\beta} \Theta_{j\beta,i\alpha} = \text{Tr}(\mathcal{H}\Theta). \quad (21)$$

Besides the bond energy, the force exerted on any atom  $i$  must be given analytically and therefore one needs the gradient of the potential energy in (18) at the position of the atom  $i$ :

$$-\mathbf{F}_i = \frac{\partial U_{\text{coh}}}{\partial \mathbf{r}_i} = \frac{\partial U_{\text{bond}}}{\partial \mathbf{r}_i} + \frac{1}{2} \sum_j^{\neq i} \frac{\partial \phi(r_{ij})}{\partial \mathbf{r}_i}. \quad (22)$$

This expression includes electronic bonds and ionic pairwise repulsions from all atoms of the system. The general form is still expensive to cope with for the simulation of mesoscopic systems.  $\mathcal{O}(N)$  scaling behavior is provided if the cohesive energy of the system is approximated by the Tersoff potential in (8), where  $b_{ij}e^{-\mu r_{ij}}$  is replaced by  $U_{\text{bond}}^{i,j}$  and a suitable cutoff with resulting balanced interatomic forces is added.

To find an efficient way to obtain the bond energy in a manner that scales linearly with the system size, too, the derivative  $\frac{\partial U_{\text{bond}}}{\partial \mathbf{r}_i}$  of the bond energy in (22) is replaced assuming a stationary electron density  $\rho$  in the electronic ground state and applying the Hellmann–Feynman theorem. The forces can now be obtained without calculating the derivatives of the electronic states and leads to the Hellmann–Feynman force [101, 102]:

$$-\mathbf{F}_i^{\text{HF}} = \sum'_{i\alpha,j\beta} \Theta_{j\beta,i\alpha} \frac{\partial H_{i\alpha,j\beta}}{\partial \mathbf{r}_i}. \quad (23)$$

Both the elements of the density matrix and the hopping elements of the Hamiltonian are functions of the relative orientation and separation of the bonding orbitals and have been calculated by *Slater* and *Koster* [103] assuming a linear combination of atomic orbitals (LCAO). To introduce the Slater–Koster matrix elements, usually denoted by  $ss\sigma, sp\sigma, pp\pi$ , etc., corresponding to the contributing orbitals and its interaction type, the TB Hamiltonian operator is transformed to a tridiagonal form. This can be done using the Lanczos transformation [104]:

$$\langle U_m \mathcal{H} \rangle U_n = a_n \delta_{m,n} + b_n \delta_{m,n-1} + b_{n+1} \delta_{m,n+1}, \quad (24)$$

$$\mathcal{H}|U_n\rangle = a_n|U_n\rangle + b_n|U_{n-1}\rangle + b_{n+1}|U_{n+1}\rangle, \quad (25)$$

where the orthonormal basis at the higher level  $n$  is recursively developed from  $|U_0\rangle$ . The coefficients  $a_n, b_n$  are the elements of the continuous fraction of the Green's function below.

The offdiagonal elements of the density matrix are related to the Green's function [105],

$$\rho_{i\alpha,j\beta} = -\frac{1}{\pi} \lim_{\eta \rightarrow 0} \Im \int^{E_f} dE G_{i\alpha,j\beta}(Z), \quad (26)$$

where the complex variable  $Z = E + i\eta$  is the real energy  $E$  with a positive, imaginary infinitesimal to perform the integration (theorem of residues). This intersite Green's function can be connected to the site-diagonal Green's function [105] via

$$G_{i\alpha,j\beta}(Z) = \frac{\partial G_{00}^A(Z)}{\partial A_{i\alpha,j\beta}} + G_{00}^A(Z)\delta_{i,j}\delta_{\alpha,\beta}, \quad (27)$$

and the latter can be evaluated recursively [106] using the coefficients of the Lanczos recursion algorithm as mentioned above:

$$G_{00}^A(Z) = \frac{1}{Z - a_0^A - \frac{(b_1^A)^2}{Z - a_1^A - \frac{(b_2^A)^2}{Z - a_2^A - \dots}}}. \quad (28)$$

The bond order can now be expressed in terms of the derivatives of the recursion coefficients  $a_n^A$  and  $b_n^A$ ,

$$\Theta_{i\alpha,j\beta} = -2 \left[ \sum_{n=0}^{\infty} \chi_{0n,n0}^A \frac{\partial a_n^A}{\partial A_{i\alpha,j\beta}} + 2 \sum_{n=1}^{\infty} \chi_{0(n-1),n0}^A \frac{\partial b_n^A}{\partial A_{i\alpha,j\beta}} \right], \quad (29)$$

with the response function  $\chi_{0m,n0}(E_f) = \frac{1}{\pi} \lim_{\eta \rightarrow 0} \Im \int^{E_f} dE G_{0m}^A(Z) G_{n0}^A(Z)$  and the elements  $G_{0n} = G_{n0}$  following from the system of equations  $(Z - a_n)G_{nm}(Z) - b_n G_{n-1,m}(Z) - b_{n+1} G_{n+1,m}(Z) = \delta_{n,m}$ . The more recursion coefficients included in (29), the more accurately the bond order will be approximated. The recursion coefficients are related to the moments of the local density of states (LDOS) [105] and the site-diagonal Green's function of (26) and (27) relates to the LDOS itself. Therefore, the recursive solution of (28) gives an approximation to LDOS in terms of its moments [107]

$$\mu_{i\alpha}^{(n)} = \int E^n n_{i\alpha}(E) dE = \sum_{\text{all } j_k \beta_k} H_{i\alpha,j_1\beta_1} H_{j_1\beta_1,j_2\beta_2} \dots H_{j_{n-1}\beta_{n-1},i\alpha} \quad (30)$$

and may be interpreted as self-returning (closed) loops of hops of length  $n$  for electrons over neighboring atoms. The local atomic environment defines the LDOS via the moments (30), which in turn is used to calculate the bond

order in (21) and the (local) atomic force (23). The remaining free parameters in the analytic form (8) with  $U_{\text{bond}}^{i,j}$  instead of  $b_{ij}$  may be fitted in the usual way. This is still a hard task, because the bond and the promotion energy involve different parameters as the repulsive part and cutoff parameters and screening functions for all terms have to be included. Besides an accurate fit, the BOP requires well-parameterized TB matrix elements or parameter optimizing, and the problem of transferability [99, 108–110] has to be considered separately. For BOP of order  $n = 2$  the bond-order term in the TS-representation reads  $b_{ij} = (-ss\sigma_{ij} + pp\sigma_{ij})\Theta_{i\sigma,j\sigma} - 2pp\pi_{ij}\Theta_{i\pi,j\pi}$  and the numerical behavior of BOP2 and TS are approximately equivalent. The details for higher-order BOP are given in the papers of Pettifor's group [2, 99]. The  $b_{ij}$  terms of the analytic BOP4 involve complex angular dependencies, partially beyond those neglected in Pettifor's formalism. For structures with defects as well as the wafer bonding of diamond surfaces where  $\pi$ -bonds cannot be neglected, BOP can be found in [111–114] and will soon be published elsewhere with detailed derivations.

## 4 Applications

It is impossible to review the rapidly growing number of successful applications of empirical MD in materials research. A few representative examples may give an impression of the wide range of problems considered. Isolated point defects are mainly simulated to check the quality of the fit of the potential parameters. Surface reconstructions, adatom and absorption phenomena, growth processes, and especially extended defect structures and interactions can be investigated in detail. The analysis of dislocation core-structures [115], the use of core-structure data for studying dislocation kink motion [116] or the dislocation motion during nanoindentation [117] are examples. Interface investigations have a long tradition, as illustrated in the standard book for grain-boundary structure [118] and growth [119]. Heterophase interfaces, e.g., using a Khor-de-Sama potential for Al and TS for SiC [120] to simulate Al/SiC interfaces, demand special attention to the correct description of the misfit [121] to get good interface energies. Simulations with the Tersoff potential and its modifications yield the correct diameter of the critical nuclei for the growth of Ge nanocrystals in an amorphous matrix [122], allow the study of growth, strains, and stability of Si- and C-nanotubes [123, 124], and SiC surface reconstructions to propose SiC/Si interface structures [125]. A review of atomistic simulations of diffusion and growth on and in semiconductors [126] demonstrates the applicability of SW and TS potentials in comparison with data from TB and DFT calculations.

In the following, two examples of our work are discussed. Empirical MD simulations of first, high-resolution electron microscopy (HREM) image contrasts in quantum dots (Sect. 4.1) and second, the physical processes at interfaces during wafer bonding (Sect. 4.2).

## 4.1 Quantum Dots: Relaxation, Reordering, and Stability

A quantum dot (QD) is a nanometer-scaled island or region of suitable material free-standing on or embedded in semiconductor or other matrices. The possibility to arrange QDs into complex arrays implies many opportunities for scientific investigations and technological applications. However, depending on the growth techniques applied (mainly MBE and MOCVD), the islands differ in size, shape, chemical composition and lattice strain, which strongly influences the confinement of electrons in nanometer-scaled QDs. The shape, size and strain field of single QDs, as well as quality, density, and homogeneity of equisized and equishaped dot arrangements determine the optical properties, the emission and absorption of light, the lasing efficiency, and other optoelectronic device properties [127, 128]. A critical minimum QD size is required to confine at least one electron/exciton in the dot. A critical maximum QD size is related to the separation of the energy levels for thermally induced decoupling. Uniformity of the QD size is necessary to ensure coupling of states between QDs. The localization of states and their stability depend further on composition and strain of the QDs. The strain relaxation at facet edges and between the islands is the driving force behind self-organization and lateral arrangement, vertical stacking on top or between buried dots, or preordering by surface structuring. In addition, an extension of the emission range towards longer wavelengths needs a better understanding and handling of the controlled growth via lattice mismatched heterostructures or self-assembling phenomena (see, e.g., [129]).

A wide variety of imaging methods are used to investigate growth, self-assembly, and physical properties of quantum dots. Among these the cross-sectional HREM and the plan-view TEM imaging techniques are suitable methods to characterize directly shape, size, and strain field [130]. But the HREM and TEM techniques images are difficult to interpret phenomenologically, especially when separating shape and strain effects. Modeling is essential to uniquely determine the features and provide contrast rules.

In Fig. 4, the atomic structure of an InGaAs-QD in a GaAs matrix (for other systems cf. [130, 131]) is prescribed by geometric models and relaxed by MD simulations. Very different dot shapes have been proposed and theoretically investigated: lens-shaped dots, conical islands, volcano-type QDs, and pyramids with different side facets of type {011}, {111}, {112}, {113}, {136}, and both {011} + {111} mixed, etc. Some of these and a spherical cap are schematically presented in Fig. 4a; in simulations one or two monolayers (ML) thick wetting layers are included, too. The most important difference between the various structures is the varying step structure of the facets due to their different inclination. There are at least two reasons to investigate these configurations [130]. First, small embedded precipitates always have facets; a transition between dome-like structure and pyramids due to changes in spacer distance, change the number and arrangement of the facets, and thus strain and electronic properties. Second, for highly faceted struc-

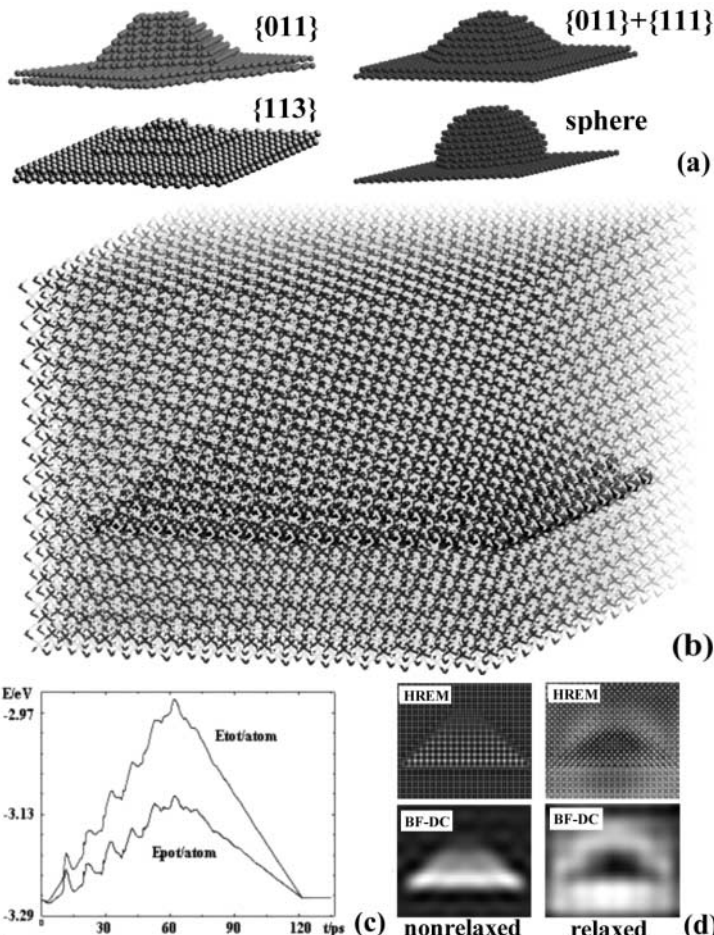


**Fig. 4.** Structure modeling and image simulation of different pyramidal-shaped quantum-dot configurations: (a) different faceting, truncation, and wetting of pyramidal start models (matrix removed, models related to (001)-base planes), (b) relaxed complete model of a {011} pyramid (base length about 6 nm,  $10 \times 10 \times 10$ -supercell length 10 nm), (c) energy relaxation of a {011} quantum dot (potential  $E_{\text{pot}}$  and total  $E_{\text{tot}}$  energy versus time steps), (d) cross-sectional HREM and bright-field diffraction contrast simulated for model (b) before and after relaxation assuming a standard 400 kV microscope at the Scherzer focus (i.e.,  $\Delta = -40 \text{ nm}$ ,  $C_s = 1 \text{ mm}$ ,  $\alpha = 1.2 \text{ nm}^{-1}$ ,  $t = 9 \text{ nm}$ ,  $\delta = 8 \text{ nm}^{-1}$ , cf. [130])

tures the continuum elasticity is practically inapplicable and finite element calculations must be done in 3-D instead of 2-D. However, the technique of ab-initio MC provides a more accurate prediction of the QD shapes than empirical MD [132]. The embedding of one perfect {011} pyramid in a matrix is demonstrated in Fig. 4b after prerelaxation. Figure 4c shows typical annealing behavior during empirical MD calculation, characterized by the potential  $E_{\text{pot}}$  and the total energy  $E_{\text{tot}}$  per atom. The energy difference  $E_{\text{tot}} - E_{\text{pot}}$  is equal to the mean kinetic energy and is thus directly related to the temperature of the system. After the prerelaxation of 5 ps at 0 K, an annealing cycle follows, 60 ps stepwise heat up to 600 K and cool down to 0 K, equilibrating the system at each heating step. The example here demonstrates a short cycle; most of the embedded QDs are relaxed at each  $T$ -step for at least 10 000 timesteps of 0.25 fs, followed by annealing up to about 900 K (the temperature is not well defined with empirical potentials but is below the melting temperature). Whereas the structure in Fig. 4b is less strained, highly strained configurations occur due to the self-interaction of the QD in small supercells that correspond to a stacked sequence with very small dot distances. The extension of the supercell chosen in the simulations depends on the extension of the QD to be investigated, as well as on the overlap of the strain fields at the borders, to avoid self-interactions. Whereas Fig. 4b shows a relatively small supercell, investigations are made for supercells of up to  $89 \times 89 \times 89$  unit cells with a base length of the QD of 9 nm containing several million atoms. For the image simulations, subregions of the supercells are used, sliced into one atomic layer and applying the multislice image simulation technique. By comparing imaging for structures before and after relaxation, Fig. 4d demonstrates the enormous influence of the relaxations on the image contrast in cross-sectional HREM and TEM [130, 131]. In summarizing some of the results one can state that MD calculations with SW (CdZnSe) and TII (InGaAs, Ge) allow us to obtain well-relaxed structures, in contrast to the static relaxations performed with the *Keating* potential [133, 134]. With this insight into the atomic processes of rearranging and straining QDs at an atomic level the growth conditions for quantum dots may be enhanced as a first step to tailoring their properties.

## 4.2 Bonded Interfaces: Tailoring Electronic or Mechanical Properties?

Wafer bonding, i.e., the creation of interfaces by joining two wafer surfaces, has become an attractive method for many practical applications in microelectronics, micromechanics or optoelectronics [135]. The macroscopic properties of bonded materials are mainly determined by the atomic processes at the interfaces (clean and polished hydrophobic or hydrophilic surfaces, as schematically shown in Fig. 5) during the transition from adhesion to chemical bonding. For this, elevated temperatures or external forces are required, as could be revealed by MD simulations of hydrogen-passivated interfaces [136]

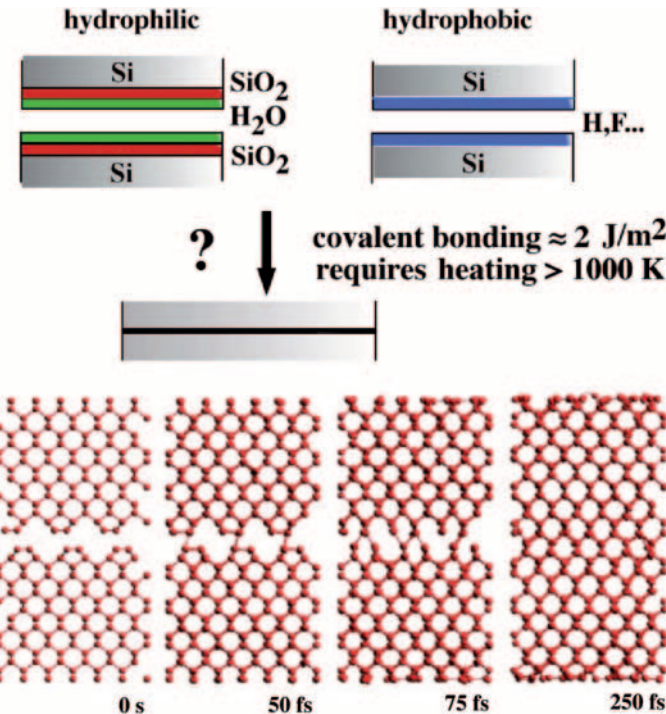


**Fig. 5.** Wafer bonding at Si[100] surfaces: simulations of surface rearrangement for perfect alignment and slow heating. The figure describes the evolution of the atomic relaxation leading to bonded wafers

or of silica bonding [65]. Thus, describing atomic processes is of increasing interest to support experimental investigations or to predict bonding behavior. Already, slightly rescaled SW potentials predict the bond behavior via bond breaking and dimer reconfiguration as shown in the snapshots explaining the possibility of covalent bonding at room temperature for very clean hydrophobic surfaces under UHV conditions [137].

Whereas the bonding of two perfectly aligned, identical wafers gives a single, perfectly bonded wafer without defects, miscut of the wafer results in steps on the wafer surfaces and edge dislocations at the bonded interfaces are created. In Fig. 6 the red color describes the potential energy above the ground state during wafer bonding over two-atomic steps. The upper terraces behave like perfect surfaces and the dimerized starting configuration of Fig. 6a is rearranged and new bonds are created. The energy gained is dissipated and for slow heat transfer the avalanche effect leads to bonding of the lower terraces, too. Two  $60^\circ$  dislocations remain and, depending on the rigid shift of the start configuration, an additional row of vacancies [137]. The dislocations may split as simulated and observed in experiments [138].

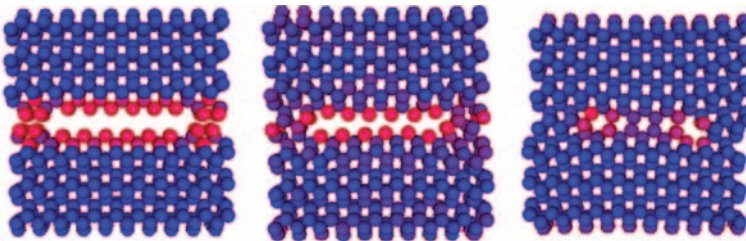


**Fig. 6.** MD simulation of wafer bonding over surface steps. Note the dislocation relaxation for the initial configuration (*left*), a snapshot during annealing up to 900 K, after 12.5 ps (*middle*) and the final relaxed state (*right*)

Bonding wafers with rotational twist leads to a network of screw dislocations at the interface. A special situation is the 90° twist, which always occurs between monoatomic steps. A Stillinger–Weber potential applied to a 90°-twist bonded wafer pair [16] yields a metastable fivefold-coordinated interface with a mirror symmetry normal to the interface characterized by a  $Pmm(m)$ -layer group (cf. Fig. 2a). Using the Tersoff or BOP-like potentials [113] and metastable or well-prepared starting configurations allows further structure relaxation and energy minimization. Figure 2b shows this relaxed configuration, which is  $(2 \times 2)$  reconstructed and consists of structural units with a  $\bar{4}2m$ - $(D2d)$  point group symmetry, called the  $\bar{4}2m$ -*dreidl*. It should be emphasized that the *dreidl* structure is found to be the minimum energy configuration also in DFT-LDA simulations [16]. However, the energies differ from those given in [139, 140]. Much more important is the modification of the band structure due to the different interface relaxation that may enable engineering of the electronic properties: whereas the metastable configuration (cf. Fig. 2c) yields semimetallic behavior, the *dreidl* structure (cf. Fig. 2d) yields a larger bandgap than in perfect lattices. The *dreidl* interface structure and its band-structure modification is very similar to the essential building blocks proposed by Chadi [141] for group-IV materials. They describe geometry and properties of the transformation of Si and Ge under pressure and the special *allo*-phases as a new class of crystalline structures.

A small misalignment of the wafers during wafer bonding yields bonded interfaces with twist rotation resulting in a checkerboard-like interface structure [142, 143]. Figure 7 shows some of the resulting minimum structures gained for higher annealing temperatures and different twist rotation angles. Before the bonding process takes place, the superposition of the two wafers looks like a Moiré pattern in the projection normal to the interface. After bonding and sufficient relaxation under slow heat-transfer conditions, almost all atoms have a bulk-like environment separated by misfit screw dislocations, which may have many kinks. The screw dislocation-network of the bonded wafer has a period half that of the Moiré pattern. One finds more imperfectly bonded regions around the screw dislocations for smaller twist

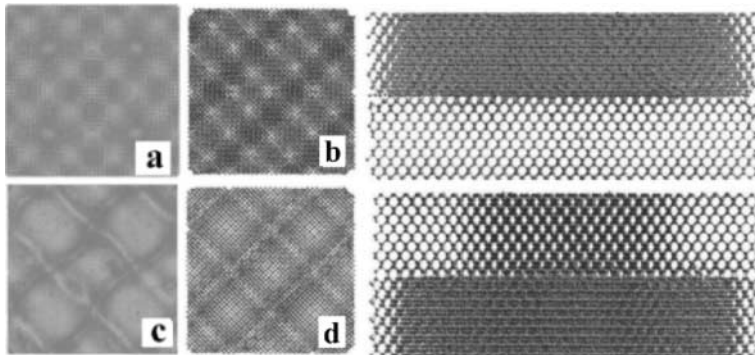


**Fig. 7.** MD relaxations of bonding rotationally twisted wafers ([001] and [110] views) with different angles: (a)  $2.8^\circ$ , 22 nm box, orthogonal dimers, [001] view; (b)  $6.7^\circ$ , 9.2 nm box, orthogonal dimers, [001] and [110] views; (c) as (a) and (d) as (b) with parallel dimers

angles, whereas bonding at higher angles results in more or less widely spread strained interface regions. In Fig. 7 bonding with orthogonal start configurations (a,b) is compared to those with parallel dimer start configurations (c,d). Thus the bonding of Figs. 7a and b may be considered as bonding with an additional  $90^\circ$  twist rotation. Clearly the periodicity of the defect region is twice those of Figs. 7b and c smoothing out the interface, but creating additional shear strains. Irrespective of the chosen twist angles and box dimensions all final structures yield bond energies of approximately 4.5 eV/atom at 0 K, however, varying slightly with the twist angle. A maximum occurs between  $4^\circ$  and  $6^\circ$  twist related to a change of the bonding behavior itself. The higher the annealing temperature the better the screw formation. In conclusion, simulation of the atomic processes at wafer-bonded interfaces offers not only the tailoring of electronic properties, it is also an important step in understanding how to control the creation of special interface structures for strain accommodation or prepatterned templates (compliant substrates) [135] by rotational alignment.

## 5 Conclusions and Outlook

Molecular dynamics simulations based on empirical potentials provide a suitable tool to study atomic processes that influence macroscopic materials properties. The applicability of the technique is demonstrated by calculating quantum-dot relaxations and interaction processes with defect creation at wafer-bonded interfaces. A brief overview describes the method itself and its advantages and limitations, i.e., the macroscopic relevance of the simulations versus the limited transferability of the potentials. The quality of the simulations and the reliability of the results depend on the coupling of the

atomistic simulations across length and timescales. Whereas the Lagrange formalism is well established for the embedding into suitable environments at the continuum level, the approximations of first-principles-based potentials need continuous future work.

## References

- [1] W. Kohn: Rev. Mod. Phys. **71**, 1253 (1999) [214](#)
- [2] M. W. Finnis: Interatomic forces in condensed matter, in *Oxford Series on Materials Modelling* (Oxford University Press, Oxford 2003) [214](#), [215](#), [221](#), [222](#), [227](#), [230](#)
- [3] K. Ohno, K. Esforjani, Y. Kawazoe: *Computational Materials Science: From ab initio to Monte Carlo Methods* (Springer, Berlin, Heidelberg 1999) [214](#)
- [4] M. C. Payne, M. P. Teter, D. C. Allen, et al: Rev. Mod. Phys. **64**, 1045 (1992) [214](#)
- [5] G. Galli, A. Pasquarello: First-principles molecular dynamics, in M. P. Allen, D. J. Tildesley (Eds.): *Computer Simulation in Chemical Physics* (Academic Publisher, Dordrecht, Netherlands 1993) pp. 261–313 [214](#)
- [6] T. Frauenheim, G. Seifert, M. Elstner, et al: phys. stat. sol. B **217**, 41 (2000) [214](#), [227](#)
- [7] D. R. Bowler, T. Miyazaki, M. J. Gillan: J. Phys.: Condens. Matter **14**, 2781 (2002) [214](#), [227](#)
- [8] J. M. Soler, E. Artacho, J. D. Gale, et al: J. Phys.: Condens. Matter **14**, 2745 (2002) [214](#), [227](#)
- [9] M. D. Segall, P. J. D. Lindan, M. J. Probert, et al: J. Phys.: Condens. Matter **14**, 2717 (2002) [214](#)
- [10] R. Car, M. Parrinello: Phys. Rev. Lett. **55**, 2471 (1985) [214](#)
- [11] G. C. Csany, T. Albaret, M. C. Payne, A. DeVita: Phys. Rev. Lett. **93**, 175503 (2004) [215](#)
- [12] P. Ruggerone, A. Kley, M. Scheffler: Bridging the length and time scales: from ab initio electronic structure calculations to macroscopic proportions, Comm. Condens. Matter Phys. **18**, 261 (1998) [215](#)
- [13] R. M. Nieminen: J. Phys.: Condens. Matter **14**, 2859 (2002) [215](#), [216](#)
- [14] R. E. Rudd, J. Q. Broughton: phys. stat. sol. B **217**, 251 (2000) [215](#), [216](#)
- [15] B. I. Lundquist, A. Bogicevic, S. Dudy, et al: Comput. Mater. Sci. **24**, 1 (2002) [215](#), [216](#)
- [16] K. Scheerschmidt, D. Conrad, A. Belov: Comput. Mater. Sci. **24**, 33 (2002) [216](#), [235](#)
- [17] J. M. Haile: *Molecular Dynamics Simulation: Elementary Methods* (Wiley, New York 1992) [216](#)
- [18] D. C. Rapaport: *The Art of Molecular Dynamics Simulation* (Cambridge Univ. Press, Cambridge 1998) [216](#)
- [19] R. Haberlandt: *Molekulardynamik: Grundlagen und Anwendungen* (Vieweg, Braunschweig, Wiesbaden 1995) [216](#)
- [20] W. G. Hoover: Molecular dynamics, in *Lecture Notes in Physics*, vol. 258 (Springer, Berlin, Heidelberg 1986) [216](#)

- [21] I. G. Kaplan: Theory of molecular interactions, in *Studies in Physical and Theoretical Chemistry*, vol. 42 (Elsevier Science Ltd., Amsterdam 1986) **216**
- [22] M. Sprik: Introduction to molecular dynamics methods, in K. Binder, G. Ciccotti (Eds.): *Monte Carlo and Molecular Dynamics of Condensed Matter Systems*, vol. 49, Conf. Proc. Vol. (SIF, Bologna 1996) Chap. 2, pp. 47–87 **216**
- [23] D. W. Heermann: *Computer Simulation Methods in Theoretical Physics* (Springer, Berlin, Heidelberg 1990) **216**
- [24] J. M. Ziman: *Principles of the Theory of Solids* (Cambridge Univ. Press, Cambridge 1972) **218**
- [25] S. W. deLeeuw, J. W. Perram, E. R. Smith: Proc. Roy. Soc. London A **373**, 27 (1980) **218**
- [26] D. Wolf, P. Kebblinski, S. R. Phillpot, J. Eggebrecht: J. Chem. Phys. **110**, 8254 (1999) **218**
- [27] A. F. Voter: Phys. Rev. B **57**, 13985 (1998) **218**
- [28] A. F. Voter, F. Montalenti, T. C. Germann: Ann. Rev. Mater. Res. **32**, 321 (2002) **218**
- [29] W. Rullmann, H. Gunsteren, H. Berendsen: Mol. Phys. **44**, 69 (1981) **221**
- [30] S. Nosé: Mol. Phys. **52**, 255 (1984) **221**
- [31] S. Nosé: J. Chem. Phys. **81**, 511 (1984) **221**
- [32] W. G. Hoover: Phys. Rev. A **31**, 695 (1985) **221**
- [33] H. C. Andersen: J. Chem. Phys. **72**, 2384 (1980) **221**
- [34] M. Parrinello, A. Rahman: J. Appl. Phys. **52**, 7182 (1981) **221**
- [35] L. Yang, D. J. Srolovitz, A. F. Yee: J. Chem. Phys. **107**, 4396 (1997) **221**
- [36] G. P. Morriss, D. J. Evans: Phys. Rev. A **35**, 792 (1987) **221**
- [37] D. J. Evans, G. P. Morriss: *Statistical Mechanics of Nonequilibrium Liquids* (Academic, London, New York 1990) **221**
- [38] J. D. Gale: Special Issue: Interatomic Potentials, Philos. Mag. B **73**, 3 (1996) **221**
- [39] A. Horsfield: Special Issue: Interatomic Potentials, Philos. Mag. B **73**, 85 (1996) **221**
- [40] S. C. Price: Special Issue: Interatomic Potentials, Philos. Mag. B **73**, 95 (1996) **221**
- [41] J. N. Murrell: Special Issue: Interatomic Potentials, Philos. Mag. B **73**, 163 (1996) **221**
- [42] D. L. Cooper, T. Thorsteinsson: Special Issue: Interatomic Potentials, Philos. Mag. B **73**, 175 (1996) **221**
- [43] M. C. Payne, I. J. Robertson, D. Thomassen, V. Heine: Special Issue: Interatomic Potentials, Philos. Mag. B **73**, 191 (1996) **221**
- [44] Guest Editor A. F. Voter, V. Vitek: MRS-Bull. **21**, 20 (1992) **221**
- [45] S. M. Foiles: MRS-Bull. **21**, 24 (1992) **221**
- [46] M. Stoneham, J. Hardy, T. Harker: MRS-Bull. **21**, 29 (1992) **221**
- [47] D. W. Brenner: MRS-Bull. **21**, 36 (1992) **221**
- [48] A. P. Sutton, P. D. Goodwin, A. P. Horsefield: MRS-Bull. **21**, 42 (1992) **221**
- [49] N. A. Marks, M. W. Finnis, J. H. Harding, N. C. Pyper: J. Chem. Phys. **114**, 4406 (2001) **222**
- [50] K. W. Jacobsen, J. K. Norskov, M. J. Puskas: Phys. Rev. B **35**, 7423 (1987) **222**
- [51] N. A. Marks: J. Phys. Condens. Matter **14**, 2901 (2002) **222**
- [52] M. S. Daw: Phys. Rev. B **39**, 7441 (1989) **222**

- [53] Y. C. Wang, K. Scheerschmidt, U. Gösele: Phys. Rev. B **61**, 12864 (2000) 222
- [54] H. R. Trebin: Comp. Phys. Commun. **121–122**, 536 (1999) 222
- [55] A. K. Rappe, C. J. Casewit, K. S. Colwell, et al: J. Am. Chem. Soc. **114**, 10024 (1992) 222
- [56] W. F. van Gunsteren, H. J. C. Berendsen: Angew. Chem., Int. Ed. Engl. **29**, 992 (1990) 222
- [57] F. H. Stillinger, T. A. Weber: Phys. Rev. B **31**, 5262 (1985) 222
- [58] R. Biswas, D. R. Hamann: Phys. Rev. B **36**, 6434 (1987) 222
- [59] T. Takai, T. Halicioglu, W. A. Tiller: Scr. Metal. **19**, 709 (1985) 222
- [60] C. P. Herrero: J. Mater. Res. **16**, 2505 (2001) 222
- [61] A. K. Nakano, B. J. Berne, P. Vashista, R. K. Kalia: Phys. Rev. B **39**, 12520 (1989) 223
- [62] S. H. Garofalini: J. Non-Cryst. Solids **120**, 1 (1990) 223
- [63] D. Timpel, K. Scheerschmidt, S. H. Garofalini: J. Non-Cryst. Solids **221**, 187 (1997) 223
- [64] D. Timpel, K. Scheerschmidt: J. Non-Cryst. Solids **232–234**, 245 (1998) 223
- [65] D. Timpel, M. Schaible, K. Scheerschmidt: J. Appl. Phys. **85**, 2627 (1999) 223, 234
- [66] M. I. Baskes: Phys. Rev. B **46**, 2727 (1992) 223
- [67] M. W. Finniss, J. E. Sinclair: Philos. Mag. A **50**, 45 (1984) 223
- [68] J. Tersoff: Phys. Rev. Lett. **56**, 632 (1986) 223
- [69] J. Tersoff: Phys. Rev. B **38**, 9902 (1989) 223
- [70] J. Tersoff: Phys. Rev. B **39**, 5566 (1989) 223
- [71] W. Dodson: Phys. Rev. B **35**, 2795 (1987) 223
- [72] G. C. Abell: Phys. Rev. B **31**, 6184 (1985) 223
- [73] D. W. Brenner: phys. stat. sol. B **217**, 23 (2000) 223
- [74] M. V. R. Murty, H. A. Atwater: Phys. Rev. B **51**, 4889 (1995) 223
- [75] D. W. Brenner: Phys. Rev. B **42**, 9458 (1990) 223
- [76] A. J. Dyson, P. V. Smith: Surf. Sci. **355**, 140 (1996) 223
- [77] K. Beardmore, R. Smith: Philos. Mag. A **74**, 1439 (1996) 223
- [78] K. Nordlund, J. Nord, J. Frantz, J. Keinonen: Comput. Mater. Sci. **18**, 504 (2000) 223
- [79] T. J. Lenosky, B. Sadigh, E. Alonso, et al: Model. Simul. Mater. Sci. Eng. **8**, 825 (2000) 223
- [80] S. D. Chao, J. D. Kress, A. Redondo: J. Chem. Phys. **120**, 5558 (2004) 223
- [81] H. Balamane, T. Halicioglu, W. A. Tiller: Phys. Rev. B **46**, 2250 (1992) 223
- [82] M. Kohyama, S. Takeda: Phys. Rev. B. **60**, 8075 (1999) 223
- [83] M. Gharaibeh, S. K. Estreicher, P. A. Fedders: Physica B **273–274**, 532 (1999) 223
- [84] S. K. Estreicher: phys. stat. sol. B **217**, 513 (2000) 223
- [85] W. Windl: phys. stat. sol. B **226**, 37 (2001) 223
- [86] S. Kohlhoff, P. Gumbsch, H. F. Fischmeister: Philos. Mag. A **64**, 851 (1991) 225
- [87] R. E. Rudd, J. Q. Broughton: Phys. Rev. B **58**, R5893 (1998) 225
- [88] A. Y. Belov: Dislocations emerging at planar interfaces, in V. L. Indenbom, J. Lothe (Eds.): *Elastic Strain Fields and Dislocation Mobility* (Elsevier, Amsterdam 1992) pp. 391–446 225, 226
- [89] J. E. Sinclair: J. Appl. Phys. **42**, 5321 (1971) 225

- [90] D. G. Pettifor: Phys. Rev. Lett. **63**, 2480 (1989) [225](#), [227](#)
- [91] C. M. Goringe, D. R. Bowler, E. Hernandez: Rep. Prog. Phys. **60**, 1447 (1997) [227](#)
- [92] A. P. Horsfield, A. M. Bratkovsky: J. Phys. Condens. Matter **12**, R1 (2000) [227](#)
- [93] D. A. Papaconstantopoulos, M. J. Mehl: J. Phys. Condens. Matter **15**, R413 (2003) [227](#)
- [94] D. G. Pettifor, I. I. Oleinik, D. Nguyen-Manh, V. Vitek: Comput. Mater. Sci. **23**, 33 (2002) [227](#)
- [95] D. Pettifor: *From Exact to Approximate Theory: The Tight Binding Bond Model and Many-Body Potentials.*, vol. 48, Springer Series (Springer, Berlin, Heidelberg 1990) [227](#)
- [96] D. G. Pettifor, I. I. Oleinik: Phys. Rev. B **59**, 8487 (1999) [227](#)
- [97] D. G. Pettifor, I. I. Oleinik: Phys. Rev. Lett. **18**, 4124 (2000) [227](#)
- [98] D. G. Pettifor, M. W. Finnis, D. Nguyen-Manh, et al: Mater. Sci. Eng. A **365**, 2 (2004) [227](#)
- [99] A. P. Sutton: *Electronic Structure of Materials* (Clarendon Press, Oxford 1994) [227](#), [230](#)
- [100] A. P. Sutton, M. W. Finnis, D. G. Pettifor, Y. Ohta: J. Phys. C **35**, 35 (1988) [228](#)
- [101] H. Hellmann: *Einführung in die Quantenchemie* (Deuticke, Leipzig 1937) [228](#)
- [102] R. P. Feynman: Phys. Rev. **56**, 340 (1939) [228](#)
- [103] J. C. Slater, G. F. Koster: Phys. Rev. **94**, 1498 (1954) [228](#)
- [104] C. Lanczos: J. Res. Natl. Bur. Stand. **45**, 225 (1950) [228](#)
- [105] A. P. Horsfield, A. M. Bratkovsky, M. Fear, et al: Phys. Rev. B **53**, 12694 (1996) [229](#)
- [106] R. Haydock: *Recursive Solution of the Schrödinger Equation*, vol. 35, Solid State Physics (Academic, London, New York 1980) [229](#)
- [107] F. Ducastelle: J. Phys. **31**, 1055 (1970) [229](#)
- [108] O. F. Sankey, D. J. Niklewski: Phys. Rev. B **40**, 3979 (1989) [230](#)
- [109] I. Kwon, R. Biswas, C. Z. Wang, et al: Phys. Rev. B **49**, 7242 (1994) [230](#)
- [110] T. J. Lenosky, J. D. Kress, I. Kwon, et al: Phys. Rev. B **55**, 1528 (1997) [230](#)
- [111] D. Conrad: *Molekulardynamische Untersuchungen für Oberflächen und Grenzflächen von Halbleitern*, Thesis, Martin-Luther-Universität, Halle (1996) [230](#)
- [112] V. Kuhlmann: *Entwicklung analytischer bond-order Potentiale für die empirische Molekulardynamik*, Thesis, Martin-Luther-Universität, Halle (2006) [230](#)
- [113] D. Conrad, K. Scheerschmidt: Phys. Rev. B **58**, 4538 (1998) [230](#), [235](#)
- [114] D. Conrad, K. Scheerschmidt, U. Gösele: Appl. Phys. Lett. **77**, 49 (2000) [230](#)
- [115] T. Harry, D. Bacon: Acta Mater. **50**, 195 (2002) [230](#)
- [116] V. V. Bulatov, J. F. Justo, W. Cai, et al: Philos. Mag. A **81**, 1257 (2001) [230](#)
- [117] E. T. Lilleodden, J. A. Zimmermann, S. M. Foiles, W. D. Nix: J. Mech. Phys. Solids **51**, 901 (2003) [230](#)
- [118] D. Wolf, S. Yip (Eds.): *Materials Interfaces: Atomic-Level Structure and Properties* (Chapman & Hall, London 1992) [230](#)
- [119] A. J. Haslam, D. Moldovan, S. R. Phillpot, et al: Comput. Mater. Sci. **23**, 15 (2002) [230](#)
- [120] X. Luo, G. Qian, E. G. Wang, C. Chen: Phys. Rev. B **59**, 10125 (1999) [230](#)

- [121] R. Benedek, D. N. Seidman, C. Woodward: J. Phys. Condens. Matter **14**, 2877 (2002) [230](#)
- [122] K. J. Bording, J. Tafto: Phys. Rev. B **62**, 8098 (2000) [230](#)
- [123] J. W. Kang, J. J. Seo, H. J. Hwang: J. Nanosci. Nanotechnol. **2**, 687 (2002) [230](#)
- [124] D. Srivasta, D. W. Brenner, J. D. Schall, et al: J. Phys. Chem. B **103**, 4330 (1999) [230](#)
- [125] C. Koitzsch, D. Conrad, K. Scheerschmidt, U. Gösele: J. Appl. Phys. **88**, 7104 (2000) [230](#)
- [126] E. Kaxiras: Comput. Mater. Sci. **6**, 158 (1996) [230](#)
- [127] D. Bimberg, M. Grundmann, N. N. Ledentsov: *Quantum Dot Heterostructures* (John Wiley & Sons., Chichester 1999) [231](#)
- [128] L. W. Wang, A. Zunger: Pseudopotential theory of nanometer silicon quantum dots, in P. V. Kamat, D. Meisel (Eds.): *Semiconductor Nanoclusters – Physical, Chemical, and Catalytic Aspects* (Elsevier, Amsterdam, New York 1997) [231](#)
- [129] H. Lee, J. A. Johnson, M. Y. He, et al: Appl. Phys. Lett. **78**, 105 (2001) [231](#)
- [130] K. Scheerschmidt, P. Werner: Characterization of structure and composition of quantum dots by transmission electron microscopy., in M. Grundmann (Ed.): *Nano-Optoelectronics: Concepts, Physics and Devices* (Springer, Berlin, Heidelberg, New York, Tokyo 2002) Chap. 3, pp. 67–98 [231, 232, 233](#)
- [131] K. Scheerschmidt, D. Conrad, H. Kirmse, R. Schneider, W. Neumann: Ultramicroscopy **81**, 289 (2000) [231, 233](#)
- [132] E. Pehlke, N. Moll, A. Kley, M. Scheffler: Appl. Phys. A **65**, 525 (1997) [233](#)
- [133] P. N. Keating: Phys. Rev. **145**, 637 (1966) [233](#)
- [134] Y. Kikuchi, H. Sugii, K. Shintani: J. Appl. Phys. **89**, 1191 (2001) [233](#)
- [135] Q. Y. Tong, U. Gösele: *Semiconductor Wafer Bonding: Science and Technology* (Wiley, New York 1998) [233, 236](#)
- [136] D. Conrad, K. Scheerschmidt, U. Gösele: Appl. Phys. Lett. **71**, 2307 (1997) [233](#)
- [137] D. Conrad, K. Scheerschmidt, U. Gösele: Appl. Phys. A **62**, 7 (1996) [234](#)
- [138] A. Y. Belov, R. Scholz, K. Scheerschmidt: Philos. Mag. Lett. **79**, 531 (1999) [234](#)
- [139] A. Y. Belov, D. Conrad, K. Scheerschmidt, U. Gösele: Philos. Mag. **77**, 55 (1998) [235](#)
- [140] A. Y. Belov, K. Scheerschmidt, U. Gösele: Phys. Status Solidi A **159**, 171 (1999) [235](#)
- [141] D. J. Chadi: Phys. Rev. B **32**, 6485 (1985) [235](#)
- [142] K. Scheerschmidt: MRS Proc. **681E**, I2.3 (2004) [235](#)
- [143] K. Scheerschmidt, V. Kuhlmann: Interf. Sci. **12**, 157 (2004) [235](#)

## Index

- |  |                                     |
|--|-------------------------------------|
| ab-initio, <a href="#">215, 216, 233</a> | algorithm, <a href="#">217, 229</a> |
| absorption, <a href="#">230, 231</a>     | alignment, <a href="#">234–236</a>  |
| adatom, <a href="#">230</a>              | amorphous, <a href="#">230</a>      |

- anharmonic, 222
- annealing, 233, 235, 236
- autocorrelation function, 224
- band structure, 216, 235
- basis set, 214
- Berendsen, 221
- Boltzmann, 219, 224
- bond order, 216, 222, 223, 228–230
- bond-order potential, 214, 215, 217, 223, 227, 230, 235
- Born–Oppenheimer, 214
- bulk modulus, 223
- canonical, 220, 224, 225
- chemical potential, 220
- classical, 213, 216, 218, 219
- cluster, 223
- cohesive energy, 218, 223, 227, 228
- concentration, 220
- conjugate gradient, 214, 215
- conservative, 217, 220
- correlation, 224
- Coulomb, 217, 218, 222
- coupling, 225, 231, 236
- covalent, 223, 234
- crack, 225
- cutoff, 217, 228
- decay, 217
- degeneracy, 228
- density matrix, 228, 229
- density of states, 227, 229
- density-functional theory, 214
- DFT, 214, 216, 222, 223, 227, 230, 235
- diamond, 230
- diffusion, 214, 224, 230
- dislocation, 230, 234, 235
- distribution function, 219
- EDIP, 222
- eigenstates, 227
- elastic embedding, 216, 220
- electron, 222, 227–229, 231
- embed, 216, 220, 225, 231, 233, 237
- embedded, 215, 216, 222, 223, 227, 231, 233
- empirical, 213–216, 222–225, 230, 233, 236
- EMT, 222
- energy level, 231
- entropy, 221, 225
- equilibrium, 222, 224, 226, 227
- ergodic, 220, 224
- Ewald, 218, 222
- exchange, 220, 228
- exchange-correlation, 214
- exciton, 231
- finite element, 214
- first principles, 214, 225, 237
- fluctuation, 221
- force, 213–217, 219, 221–223, 226–228, 230, 231, 233
- Fourier, 225
- free energy, 224, 225
- Ge, 223, 230, 233, 235
- general gradient approximation, 214
- GGA, 214
- Gibbs, 219, 220, 225
- glass, 223
- grain boundary, 230
- grand-canonical, 220, 225
- Green’s function, 227, 229
- Green–Kubo, 224
- ground state, 228, 234
- Hamiltonian, 218–220, 227, 228
- handshaking, 215, 219, 225
- Heisenberg, 219
- Hellmann–Feynman, 214, 228
- heterostructure, 231
- hopping, 228
- hybrid, 222
- hydrogen, 233
- imaginary, 229
- interface, 215, 216, 225, 230, 233–236
- internal energy, 224
- isothermal, 224
- jellium, 222
- kink, 230
- Lagrange, 219, 221, 237
- Lagrangian, 218, 219, 221, 225–227
- LDA, 214

- Lennard-Jones, 222
- Liouville, 219
- liquid, 219
- localization, 213, 217, 231
- Madelung, 218, 222
- Maxwell, 221
- melting, 233
- microcanonical, 217, 220, 221, 225
- misfit, 230, 235
- molecular dynamics, 213, 216
- Morse, 222
- multipole, 223, 226
- nanometer, 231
- Newton, 227
- Nosé, 221
- optical, 231
- optoelectronic, 231
- pair-distribution function, 220, 224
- Parrinello, 221
- partition function, 219, 224
- periodic boundary conditions, 220
- periodicity, 236
- perturbation, 221, 222
- phase space, 219, 220
- phonon, 223, 226
- point defect, 223, 230
- potential, 214–218, 220–223, 225–228, 230, 233–235
- precipitates, 231
- pseudoatom, 222
- pseudopotential, 214, 222
- quantum dot, 225, 230, 231, 233, 236
- radial-distribution function, 224
- recursion, 227, 229
- relaxation, 215, 216, 231, 233, 235, 236
- repulsive, 222, 230
- rotational, 235, 236
- scattering, 225
- screening, 218, 222, 230
- self-interaction, 217, 233
- self-organization, 231
- semiempirical, 216, 223
- shear, 224, 236
- Si, 222, 223, 230, 235
- Siesta, 214
- Slater, 227, 228
- spherical harmonic, 223
- spin degeneracy, 228
- statistical, 216, 219, 224
- Stillinger–Weber, 222, 235
- strain, 221, 224, 225, 230, 231, 233, 236
- stress, 221, 224
- supercell, 220, 233
- surface, 215, 216, 220, 230, 231, 233, 234
- symmetric, 221
- symmetry, 235
- Taylor, 217, 222
- temperature, 218, 221, 224, 233–236
- Tersoff, 223, 228, 230, 235
- thermostat, 220, 221
- tight binding, 214, 215, 222
- total energy, 217, 220, 233
- trajectory, 219, 220
- transferability, 222, 230, 236
- transition, 217, 218, 222, 228, 231, 233
- transport, 221, 224
- Van der Waals, 222
- variational, 218
- velocity autocorrelation, 224
- Verlet, 217
- wafer bonding, 215, 230, 233–235
- water, 223
- wavelength, 231
- X-ray, 225

